Available online at www.sciencedirect.com
SCIENCE DIRECT
Polymer 46 (2005) 7759–7770
polymer
www.elsevier.com/locate/polymer

Gel machines constructed from chemically cross-linked actins and myosins

Akira Kakugo[a], Kazuhiro Shikinaka[a], Jian Ping Gong[a,b,*], Yoshihito Osada[a]

[a]*Biological Sciences, Graduate School of Science, Hokkaido University, Sapporo 060-0810, Japan*
[b]*SORST, JST, Sapporo 060-0810, Japan*

Received 28 January 2005; accepted 7 February 2005
Available online 13 June 2005

Abstract

We report an ATP fueled soft gel machine reconstructed from muscle proteins of actin and myosin. Chemically cross-linked actin gel filaments, several decade times the length of native actin filaments (F-actin) move along a chemically cross-linked myosin fibrous gel (1 cm long and 50 μm in diameter) with a velocity as high as that of native F-actin, by coupling to ATP hydrolysis. The motility observed in muscle protein-gels suggests that one might reconstruct a soft machine fueled by chemical energy by using actin and myosin molecules as elementary elements.

Keywords: Polyioncomplex; Polarity; Motility

1. Introduction

There are two basic differences between the motion in a man-made machine and in a biological motor. One is in their principles. The motion of a man-made machine, which is constructed from hard and dry materials such as metals, ceramics or plastics, is realized by the relative displacement of the macroscopic constituent parts of the machine. In contrast to this, the motion of a living organism, which consists of soft and wet protein and tissues, is caused by a molecular deformation that is integrated to a macroscopic level through its hierarchical structure [1–3]. The other is in their energy sources. The man-made machine is fueled by electrical or thermal energy with an efficiency of around 30%, but a biological motor is driven by direct conversion from chemical energy with an efficiency as high as 80–90% [4].

In order to create biomimetic systems, polymer gels have been employed due to their reversible size and shape change, thereby realizing the motion by integrating the deformation on a molecular level. Over the past number of years, using these idea several kinds of artificial soft machines have been constructed using synthetic polymer gels. Examples include Gelooper (gel-looper), gelf (gel golf), gel valves, chemical motor, etc. [5–11]. However, the lack of hierarchical structures and energy sources inside the gel lead to a decreased response and restricts the further application of such actuators for practical use in the human body.

Recently, we have found that chemically cross-linked giant actin gel filaments, several tens of times the length of native actin filaments, move along a chemically cross-linked myosin fibrous gel with a velocity as high as that of native actins, by coupling to ATP hydrolysis [12–15] (Actins and myosins are major component of muscle proteins and play an important role in dynamic motion of creatures that is caused by the molecular deformation using the chemical energy released by hydrolysis of ATP). This result indicates that muscle proteins can be tailored into desired shape and size without sacrificing their bioactivities.

In this article we will describe the adenosine triphosphate (ATP) fueled soft gel machine constructed from chemically cross-linked actin gel and myosin gel.

* Corresponding author. Address: Biological Sciences, Graduate School of Science, Hokkaido University, Sapporo 060-0810, Japan. Tel./fax: +81 11 706 2774.
E-mail address: gong@sci.hokudai.ac.jp (J.P. Gong).

0032-3861/$ - see front matter © 2005 Elsevier Ltd. All rights reserved.
doi:10.1016/j.polymer.2005.02.124

2. Methods

2.1. Materials

2.1.1. Sample preparation

Actin was obtained from scallops by the method of Spudich and Watt [16]. Myosin was obtained from scallops by the method of Barany et al. [17]. Heavy meromyosin (HMM) was obtained by the method of Craig et al. [18]. Cationic polymers (*x*,*y*-ionene (*x* = 3 or 6; *y* = 3, 4, or 10) bromide polymers (*x*,*y*-ionene), poly-L-lysine hydrochloride (*p*-Lys), poly-*N*-[3-(dimethylamino)propyl]-acrylamide (PDMAPAA-Q)) and other polymer (poly <ce:small-caps>l-glutamic acid sodium salt (*p*-Glu), deoxyribonucleic acid sodium salt (DNA), polyethylene glycol (PEG))were prepared as described in previous papers [13,15].

2.1.2. Oriented myosin gel preparation

Myosin (10 mg/ml) dissolved in 50 mM 3-(*N*-morpholino)propanesulfonic acid (MOPS; pH 7.0) containing 600 mM KCl was spread on the slide glass plate and then dipped into 50 mM MOPS (pH 7.0) containing 10 mM KCl for 10 min at 4 °C keeping the angle of slide glass to water surface as 60° to the water surface. Part of the film edge was slowly picked up using tweezers, stretched with a velocity of 3–4 mm/s, and dipped in TG solution (1 unit against 1 mg myosin) for 30 min at 13 °C to give chemical cross-links. The cross-linked myosin filament was rinsed in 50 mM MOPS (pH 7.0) containing 600 mM KCl for several hours to remove soluble myosin.

2.1.3. Polymer–actin complex preparation

Fluorescent-labeled actin filaments (denoted as F-actin) were obtained by stoichiometrically mixing G-actins and rhodamine–phalloidin (Molecular Probes No. 4171) in F-buffer (5 mM *N*-2-hydroxyethylpiperazine-*N*′-2-ethanesulfonic acid (HEPES; pH 7.2), 0.2 mM ATP, 0.2 mM $CaCl_2$, 100 mM KCl, 2 mM $MgCl_2$) for 24 h at 4 °C. Phalloidin bonds to G-actin stoichiometrically and stabilizes the F-actin against de-polymerization at a decreased critical concentration of actin.

The polymer–actin complex was obtained by mixing F-actin that was diluted to 0.001 mg/ml with F-buffer and various kinds of polymers with a prescribed weight ratio of [polymer]/[F-actin] at room temperature.

2.2. Mg-ATPase activity

The actin activated Mg-ATPase activity was measured by determining the amount of inorganic phosphate liberated from ATP for 8 min at 15 °C (50 mM KCl, 20 mM Tris (pH 7.4) containing 2 mM $MgCl_2$, 0.3 mM $CaCl_2$ and 1 mM ATP) in the presence of myosin gels (0.66 mg/ml) and 0.5 wt% native actin, or actin gels in the absence of monomeric actins and myosins. The reaction was terminated by adding 10% of trichloroacetic acid (TCA). The liberated inorganic phosphate was determined by the method of Youngburg and Youngburg [19].

2.3. Electron microscopy

Transmission electron microscopy (TEM) was performed by using a JEOL (JEM-1200EX) at 120 kV acceleration voltage. A drop of F-actin–polymer mixture of about 10 μl was put on carbon-coated 200-mesh grids that were rendered hydrophilically by glow discharge in a reduced pressure. After waiting for 180 s for adsorption, the grids were stained by one drop of phosphotungstic acid (pH 7.2).

2.4. Motility assay [20–22]

The polymer–actin complex was obtained by mixing F-actin that was diluted to 0.001 mg/ml with F-buffer and various kinds of polymers with a prescribed weight ratio of [polymer]/[F-actin] at room temperature: [*p*-Lys]/[actin] = 0.35 g/g, [PDMAPAA-Q]/[actin] = 0.49 g/g, [3,3-ionene]/[actin] = 4.1 g/g, [6,4-ionene]/[actin] = 0.54 g/g, [6,10-ionene]/[actin] = 0.74 g/g.

The polymer–actin complex gel was obtained from F-actin solution containing 20 mM KCl, 10 mM dithiothreitol (DTT), 5 mM $MgCl_2$, 0.1 mM $CaCl_2$, 10 mM MOPS (pH 7.2), and 25% glutaraldehyde solution (Junsei Chem Co., Tokyo, Japan) as the cross-linker in the presence of polycation (750 unit/mol). After cross-linking at 15 °C for 1 h, the polymer–actin complex gel was obtained by adding 2-mercaptoethanol for termination of reaction.

Myosin (1 mg/m1) was placed on a cover glass that was pre-coated with 0.03% nitrocellulose. The cover glass was then placed on a slide glass equipped with spacers 1.1–1.4 mm high placed at both sides. The flow-cell made in this way was filled with 50 mM MOPS (pH 7.0) buffer and placed on ice. The flow cell was washed with 600 mM KCl and 50 mM MOPS (pH 7.0) and was then filled with buffer (50 mM KCl, 25 mM DTT, 2 mM $MgCl_2$, 0.3 mM $CaCl_2$ and 30 mM imidazole (pH 7.6)) containing 0.3 wt% methylcellulose. A total of 2 μl of F-actin and polymer–actin complex gel in the assay buffer was introduced into the flow cell. The cell was placed on the stage of a fluorescence microscope (Olympus BX 50), and the fluorescent-labeled F-actins were observed using a 60× objective. The movement of F-actin and polymer–actin complex gel was initiated by filling the cell with assay buffer containing a prescribed amount of ATP at 20 °C. The fluorescent image was obtained with an inverted charge-coupled device camera (Olympus Color Camera HCC-3900) and recorded on a video recorder (Digital Videocassette Recorder DSR-30). The velocity of F-actins or polymer–actin complex gel on the surface of myosin was evaluated by the displacement of their center position in 3.3 s. The motility assay on oriented myosin gel was carried out in the same method.

2.5. Polarity measurement

A drop of polymer–actin (obtained by the method of Brown and Spudich [23]) mixture of about 10 μl was placed on carbon-coated 200-mesh grids that were coated by molten dental wax. After waiting for 10∼40 s for adsorption, two drops of HMM buffer were placed on the grid to remove excess polymer–actin mixture. And then one drop of HMM (0.1 to 0.5 mg/ml in HMM buffer) was placed on the grid. After waiting for 10–20 s, the grids were washed by eight drops of 10 mM-NaPi (pH 7.2). After washing, the grids were stained by four drops of 1% (w/v) uranyl acetate (pH 4.0). Samples were observed with a JEM-1200EX microscope (JEOL, Tokyo, Japan) at a 120 kV acceleration voltage. The polarity of the polymer–actin complex was defined by the following equation

$$\text{polarity} = \frac{|n_1 - n_2|}{n_1 + n_2} \quad (1)$$

where n_1 and n_2 are the numbers of actin filaments pointing in the two perpendicular directions. Polarity was the average over about 20 samples.

3. Results

3.1. Actin gel formed from polymer–actin complexes [13]

Since, the isoelectric point of actins is pH 4.7, F-actins in neutral buffer are negatively charged. Therefore, they were assumed to form complexes with cationic polymers through electrostatic interaction. Fig. 1(a)–(d) shows some examples of fluorescence microscope images of polymer–actin complexes obtained by mixing F-actins with *p*-Lys (Fig. 1(a)) and *x*,*y*-ionene polymers (Fig. 1(b)–(d)) for 120 min. One can see that large filamentous, stranded and branched complexes of 20–30 μm in size are formed in the presence of *p*-Lys, 3,3- 6,6- 6,12-ionene polymers and their morphological nature, both of size and shape, are strongly in contrast to that of native F-actin (Fig. 1(e)). Fig. 2(a) shows time courses of the average length of the complexes in the presence of various kinds of polymers. Polymers have been mixed with following weight ratios keeping the actin concentration constant at 0.001 mg/ml as well as the molar ratio of ammonium cation of polymer to actin monomer of F-actin as 100:1 for *p*-Lys and 30:1 for ionene polymers: [*p*-Lys]/[actin]=0.35 g/g, [3,3-ionene]/[actin]=0.41 g/g, [6,4-ionene]/[actin]=0.54 g/g, [6,6-ionene]/[actin]=0.61 g/g, [6,10-ionene]/[actin] =0.74 g/g, [6,12-ionene]/[actin]=0.81 g/g.

The number-average length of fluorescence image of F-actins is 2.14 μm with a standard deviation of 0.11 μm

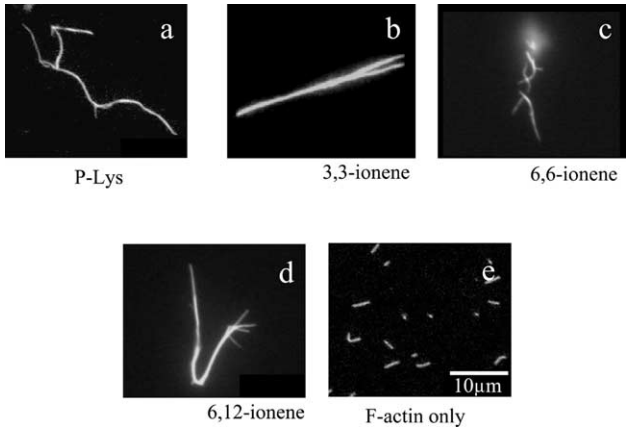

Fig. 1. Fluorescence microscope images of polymer–actin complexes formed by mixing F-actin and various cationic polymers at room temperature. (a) *p*-Lys, (b) 3,3-ionene, (c) 6,6-ionene, (d) 6,12-ionene, (e) F-actin only. The molar ratio of ammonium cation of polymer to monomeric actin was kept constant at 30:1 for *x*,*y*-ionene polymers and 100:1 for *p*-Lys, which corresponding to weight ratios of [3,3-ionene]/[actin]=0.41 g/g, [6,6-ionene]/[actin]=0.61 g/g, [6,12-ionene]/[actin]=0.81 g/g, [*p*-Lys]/[actin]=0.35 g/g. Actin concentration was 0.001 mg/ml ([13]).

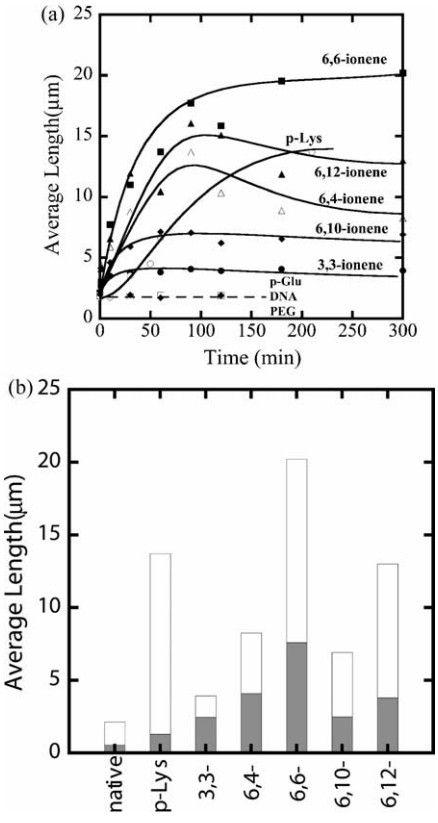

Fig. 2. (a) Time courses of polymer–actin complexes growth. (b) Average length of polymer–actin complexes observed from fluorescence microscope images (white columns) and from transmission electron microscope (TEM) images (shade columns) at 210–300 min. The molar ratio of ammonium cation to monomeric actin was 30:1 for *x*,*y*-ionene polymers and 100:1 for *p*-Lys. The corresponding weight ratios were as follows: [3,3-ionene]/[actin]=0.41 g/g, [6,4-ionene]/[actin]=0.54 g/g, [6,6-ionene]/[actin]=0.61 g/g, [6,10-ionene]/[actin]=0.74 g/g, [6,12-ionene]/[actin]=0.81 g/g, [*p*-Lys]/[actin]=0.35 g/g, [*p*-Glu]/[actin]=0.36 g/g, [DNA]/[actin]=0.77 g/g, [PEG]/[actin]=0.10 g/g. Actin concentration: 0.001 mg/ml [JPG2] ([13]).

(average over 784 samples) in the F-buffer. However, polymer–actin complexes grow with time and reach as large as 5–20 μm within 1 or 2 h, which is about 2–10 times larger than that of native F-actin. The growth profiles depend on the chemical structure of the polycations. *p*-Lys shows a relatively slow growth profile but gives out a large complex. On the other hand, 3,3-ionene polymer gives the smallest complexes. These results indicate that hydrophobicity and charge density of the ionene polymers are important in complex formation. The average lengths of polymer–actin complexes are shown in Fig. 2(b). To confirm that this kind of actin growth is due to the complex formation via electrostatic interaction between the negatively charged actins and positively charged polymers, we further studied the actin growth in the mixture solution of actins and negatively charged polymers such as *p*-Glu, DNA, and neutral polymer, such as PEG at a molar ratio of monomeric units of polymer to F-actin of 100:1. As shown in Fig. 2(a), the F-actins do not grow into large filaments with time in the presence of these anionic or neutral polymers. Therefore, the formation of polymer–actin complexes should be attributed to the electrostatic interaction between actins and cationic polymers. As shown in Fig. 2(a), although 3,3-ionene has a similar high charge density as that of *p*-Lys that has charged moiety on its side chain, it shows a much less ability of complex growth. This indicates that although the complex formation is initiated by the electrostatic interaction, the flexibility of the charged moiety is important. The complicated *x*, *y* value dependence of the complex growth observed in *x*,*y*-ionene polymers might be associated with the complementary effect between the charge density and the flexibility of the charged moiety. Both 3,3-ionene and 6,10-ionene form short complexes because the former has a high charge density but with a less flexibility, while the latter has a high flexibility but with a low charge density. 6,6-Ionene gives longest complex due to its proper charge density and flexibility. Here, we could not find a clear role related to the hydrophobicity of the *x*,*y*-ionene polymers. The decrease in the filament length after 100 min of complex formation observed for 6,4- and 6,12-ionene complexes seems to be due to the aggregation of the complex.

Since, the formation of polymer–actin complexes is an equilibrium reaction, the morphological features of the product should depend not only on time and polymer structure, but also on concentrations of actins and polymers. Fig. 3(a) shows the effect of actin concentration on the equilibrium size of the polymer–actin complexes when mixed with *p*-Lys of a constant concentration (3.5×10^{-4} mg/ml). When the actin concentration exceeds 0.001 mg/ml, the polymer–actin complexes increase the length steeply with the increase in the concentration and then saturate to a length around 15–20 μm. Fig. 3(b) shows the effect of *p*-Lys concentration on the relative length β of polymer–actin complexes in the equilibrium at a constant actin concentration (0.001 mg/ml). Here β is defined as a ratio of average length to maximum length of actin–polymer

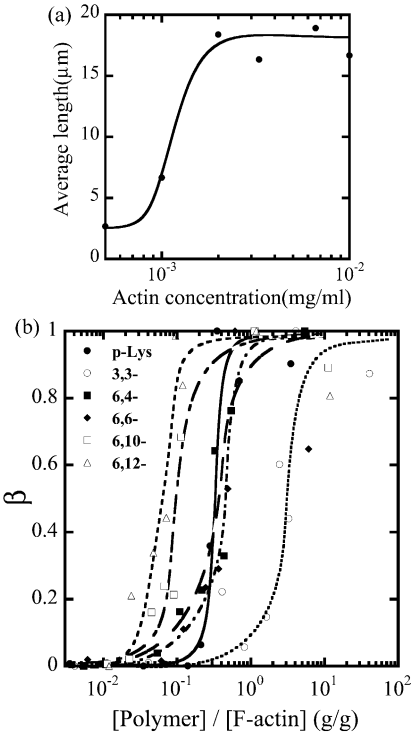

Fig. 3. Average length of polymer–actin complexes as a function of F-actin concentration (a) and dependence of β on the mixing ratio of polymer to actin (b). Here β is defined as the ratio of average length to maximum length of actin–polymer complex. Data in (a) were obtained at [*p*-Lys] = 3.5×10^{-4} mg/ml at 60 min. and in (b) at an actin concentration of 0.001 mg/ml at 90 min ([13]).

complex. No actin growth is observed at all when the mixing ratio of *p*-Lys to actin is lower than 0.14 g/g, indicating that the polymer–actin complex does not form at such a low concentration. However, the length of polymer–actin complexes abruptly increases when the mixing ratio of *p*-Lys to F-actin exceeds 0.21 g/g. Thus, there exists a critical *p*-Lys concentration to form complex, indicating that the complex formation is cooperative. The similar cooperative behavior was also observed in the complex formation with ionene polymers, and the critical mixing ratios of 3,3- 6,4- 6,6- 6,10- and 6,12-ionene to F-actin were about 0.81, 0.054, 0.12, 0.024, and 0.022 g/g at a constant F-actin concentration (0.001 mg/ml), respectively (Fig. 3(b)). These results explain why we observed a shortest complex length of 3,3-ionene in Fig. 2(a) performed at [3,3-ionene]/[actin] = 0.41 g/g, which was less than the critical value of 0.81 g/g. Now, we can conclude that interaction between polymers and actins behave cooperatively, and polymer–actin complexes are formed only when both F-actin concentration and the mixing ratio exceed the critical values.

From Fig. 3(b) we can obtain the binding constant (K) as well as the other thermodynamic parameters of the actin–polymer interaction by the following equation [24–26]. $K = K_0 u = 1/(\mathrm{Cs})_{0.5}$, where K_0 is the binding constant of the cationic polymer bound to an isolated binding site on the

actin filament (initiation process), $(Cs)_{0.5}$ is the cationic polymer concentration at $\beta = 0.5$, here β is defined as a ratio of average length to maximum length of actin–polymer complex, and u is the cooperative parameter which tells the extra interaction energy between the binding sites (propagation process). The value of u can be calculated from the slope of the growth profile at the half-length point

$$\left(\frac{d\beta}{(d \ln Cs)_{0.5}}\right) = \frac{\sqrt{u}}{4} \quad (2)$$

K_0 and u as well as the total binding energy ($\Delta F_{total} = -RT \ln K$) and cooperative energy change ($\Delta F_{coop} = -RT \ln u$) were calculated and the results are summarized in Table 1. One can see a large value of the cooperative parameter (u) and, therefore, a large cooperative energy (ΔF_{coop}) change for *p*-Lys and 3,3-ionene, and the smallest value of cooperative parameter is observed for 6,12-ionene, which is one order of magnitude smaller than the value of the other polymers. On the contrary, 6,12-ionene shows the highest binding constant of the initiation process (K_0).

As the lateral structures of the polymer–actin complexes are too small to be clearly observed by fluorescent optical microscope, we further studied polymer–actin complexes by TEM, using the negative staining technique. Fig. 4 shows the TEM images of the actin complexes prepared at a molar ratio of ammonium cation of polymer to monomeric actin as 100:1 for *p*-Lys and 30:1 for ionene polymers at a constant F-actin concentration 0.001 mg/ml. As shown in Fig. 4(a), actin forms a relatively homogeneous and thin filament in the presence of *p*-Lys. We also found that actin is able to form an extremely homogeneous nano-scale wire (nano-wire) with 3,3-ionene (Fig. 4(b)). Filamentous complexes are observed in the presence of 6,6-ionene, (Fig. 4(c)). Occasionally ring shaped complex (nano-ring) is observed in 6,6-ionene-actin complex (Fig. 4(d)).

The average width of 3 the *p*-Lys-actin complex is 21.0 nm with a standard deviation of 2.6 nm. Comparing with the native F-actins that have an average width of 12.1 nm with a standard deviation of 1.2 nm, *p*-Lys-actin complexes are only slightly thicker than that of the native F-actin with almost the same width scattering. 3,3-ionene complexes also showed a very thin and homogeneous wire-like morphology showing an average width of 16.1 nm with a standard deviation of 1.7 nm. However, from Fig. 3(b), we know that at a molar ratio of ammonium cation to actin monomer as 30:1, the 3, 3-ionene polymer concentration is still below the critical concentration. Since, the complex morphology is strongly dependent on the polymer concentration, we further investigated the 3,3-ionene-actin complex at a molar ratio of ammonium cation to actin monomer as 300:1 ([3,3-ionene]/[actin] = 4.1 g/g), which is above the critical concentration of complex formation. As shown in Fig. 4(e), bundles of thin filaments are formed when the 3,3-ionene polymer exceeds the critical concentration. Similar morphology are observed for other *x*,*y*-ionene polymers above their critical concentration. Actin-6,4-, 6,6-, 6,10-, and 6,12-ionene complexes have an average width of 79.0, 59.3, 38.7 and 66.1 nm with a standard deviation of 60, 29, 21, and 27 nm, respectively (Fig. 5). The large scattering in the width of actin-6,4-, 6,6-, 6,10-, and 6,12-ionene complexes quantitatively indicates the randomness of the morphology of the complexes.

Thus, designed micro-order polymer–actin complexes could be obtained by changing the structure of cationic polymer and other conditions. The polymer–actin complexes were chemically cross-linked with the cross-linking reagents (refer to experimental section) to form stable gels (hereafter called, polymer–actin complex gel). The motility of these polymer–actin complex gels will be described in Section 3.2.

3.2. Oriented myosin gel formed by shear stress [12,14]

The chemically cross-linked myosin gel with its oriented filament array 1 cm long and 50 μm in diameter was obtained by reacting the scallop myosin at pH 7.0 using transglutaminase (TG) under stretching. The oriented myosin gel is semi-transparent, showing a swelling degree of ca. 100, and a Young modulus of 190 Pa in the oriented direction, which is more than two times larger than that of the myosin gel prepared without stretching. Fig. 6(a) and (b) show scanning electron microscopy (SEM) and atomic force microscopy (AFM) images of an oriented myosin gel, respectively. Distinct bundles of regularly oriented filaments ca. 1.5 μm in diameter are observed, indicating that the rod-like myosin molecules are self-organized with orientation to form a hierarchical structure as schematically shown in Fig. 6(c). The molecular orientation of filaments was confirmed by the strong IR dichroism of carbonyl absorption at 1600 cm^{-1}, which could not be observed in the absence of stretching.

The chemically cross-linked myosin gel showed an

Table 1
Thermodynamic interaction parameters of complex formation between F-actin and various cationic polymers [JPG3] ([13])

Polymer	K (10^6)	u	K_0 (10^5)	ΔF_{total} (kJ/mol)	ΔF_{coop} (kJ/mol)
p-Lys	3.9	31	1.2	−37	−8.4
3,3-	0.4	32	0.1	−31	−8.4
6,4-	2.9	4.4	6.6	−36	−3.5
6,6-	2.3	20	1.2	−36	−7.3
6,10-	10.6	7.0	1.5	−39	−4.7
6,12-	15.3	2.2	7.1	−40	−1.9

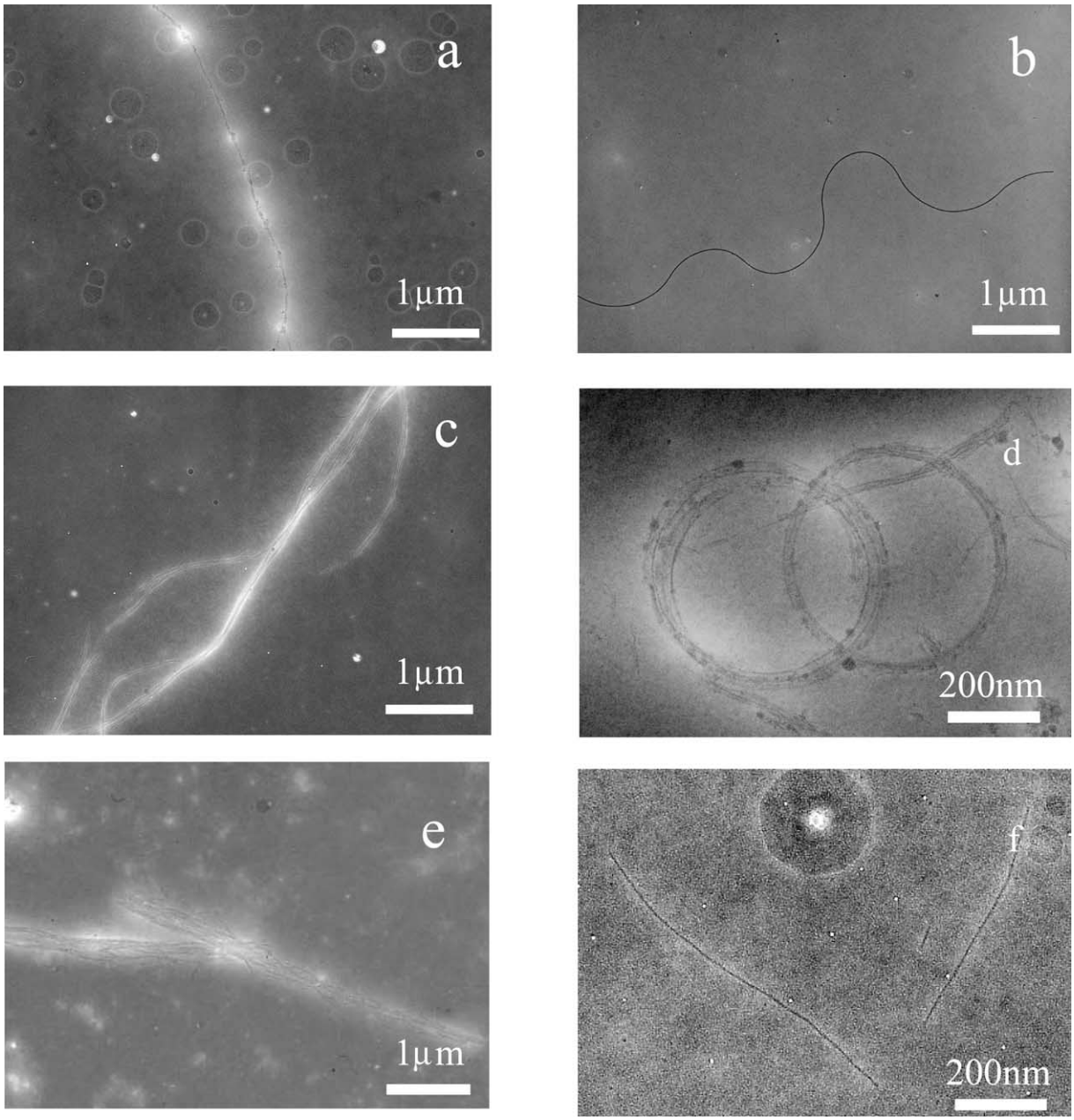

Fig. 4. Transmission electron microscope (TEM) images of polymer–actin complexes formed by mixing F-actin and various polymers at room temperature for 240 min. (a) *p*-Lys (b) 3,3-ionene, (c) 6,6-ionene (d) 6,6-ionene (e) 3,3-ionene (f) F-actin only. Mixing molar ratios are 100:1, the same as fluorescence microscope observation (Fig. 1), except for (e) which is carried out at 300:1 ([3,3-ionene]/[actin] = 4.1 g/g). Actin concentration: 0.001 mg/ml ([13]).

ATPase activity as high as that of native myosins in the presence of 0.5 w/w native actin. Myosin gels cross-linked by other cross-linking agents, such as glutaraldehyde and 1-ethyl-3-(3dimethyl aminoprolyl)carbodiimide, also showed an ATPase activity, though not as high as those cross-linked by TG. These results encouraged us to investigate the motility of native F-actin on the myosin gel.

3.3. Motility assay of F-actin

As shown in Fig. 7, the average velocity, calculated from the mean displacement over 30–50 samples of F-actin in 3 s, sharply increased with an increase in ATP concentration, and the profiles were essentially the same as that on native myosins. A reciprocal plot of velocity against ATP concentration (Lineweaver–Burk plot) showed a liner relationship for the myosin gel, indicating essentially the same ATP coupling process takes place as for a native myosin.

F-actins showed a preferential motion along the axis of oriented myosin gel as elucidated by the degree of anisotropy (DA), which is defined as the ratio of the square-root average velocity in the fiber direction to that perpendicular to the fiber direction. The DA measured on

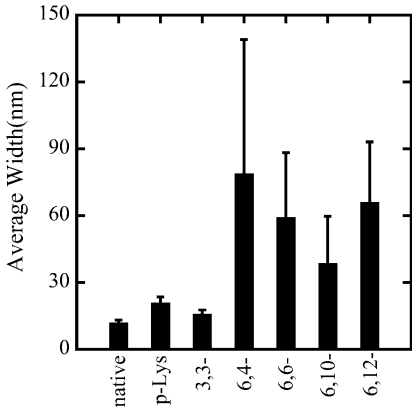

Fig. 5. Average width of polymer–actin complexes obtained at 240 min by TEM images. Error bar means standard deviation ([13]).

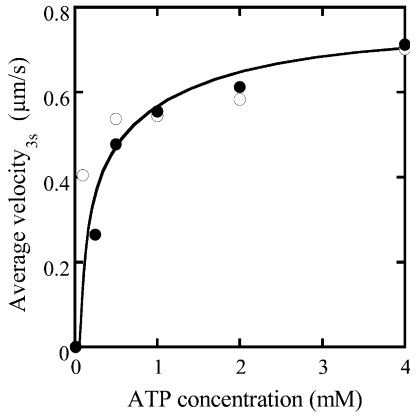

Fig. 7. Mean average velocity of native F-actin on the chemically cross-linked myosin gel (opened circle) and on native myosin (closed circle), as a function of ATP concentration. Plots represent mean velocity over 30–50 F-actins ([12]).

the non-oriented myosin gel was 1.1 (average over 66 samples), and that on the oriented myosin gel was 1.7 (average over 91 samples). The mean velocity on the non-oriented myosin gel was 0.69 μm/s with a standard deviation of 0.24 μm/s, while that on the oriented myosin gel was 0.83 μm/s with a standard deviation of 0.30 μm/s. Thus, actin filaments prefer to move along the axis of the oriented myosin gel with an increased velocity.

3.4. Motility assay of polymer–actin complex gel

The *p*-Lys-actin complex gel cross-linked with TG also showed a high motility on the oriented myosin gel in spite of its large dimension. As shown in Fig. 8(a), the *p*-Lys-actin complex gels moved preferentially along the axis of oriented myosin gel almost without path deviations. Fig. 8(b) shows the velocity distributions of *p*-Lys-actin complex gels on the oriented myosin gel (closed circles) as a function of the individual filament size. The *p*-Lys-actin complex gels, about four times larger than native F-actin, moved with an average velocity of 1 μm/s, almost the same as that of native F-actins on the oriented myosin gel (opened circles). Some of the *p*-Lys-actin complex gels moved as fast as 2.0 μm/s. In addition, DA of the *p*-Lys-actin complex gels was 2.2 (average over 38 samples) on the oriented myosin gel, which was higher than that of the native F-actin (DA = 1.7), indicating an enhanced directional preference along the axis of the oriented myosin gel.

Thus, despite its increased mass, the *p*-Lys-actin complex gel, several tens to hundreds times the volume of

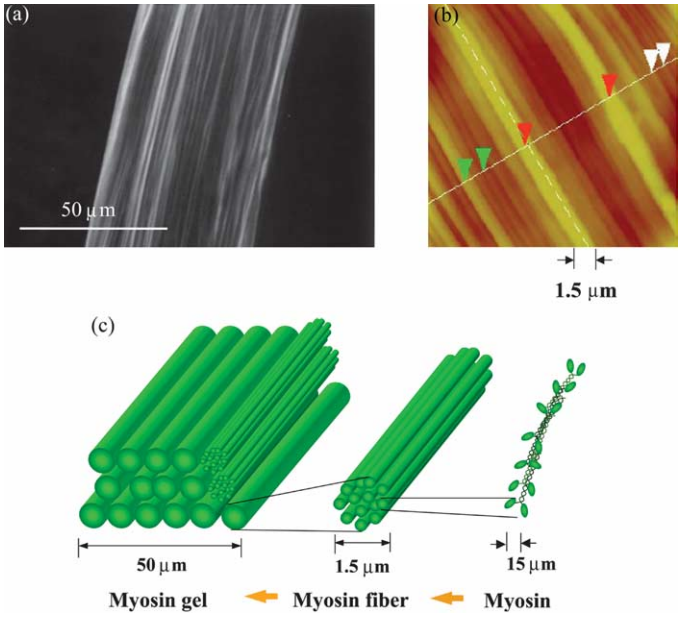

Fig. 6. (a) Scanning electron microscope (SEM) image and (b) atomic force microscope (AFM) image of the oriented myosin gel chemically cross-linked by TG under stretching. (c) Hierarchical structure of oriented myosin gel. The myosin gel fiber, ca. 1 cm long and 50 μm in diameter, is an aggregate of ca. 1000 bundles 1.5 μm in diameter. Since, a rod-like myosin molecule is 15 nm in diameter, one bundle has a diameter of 10^4 myosin molecules ([12]).

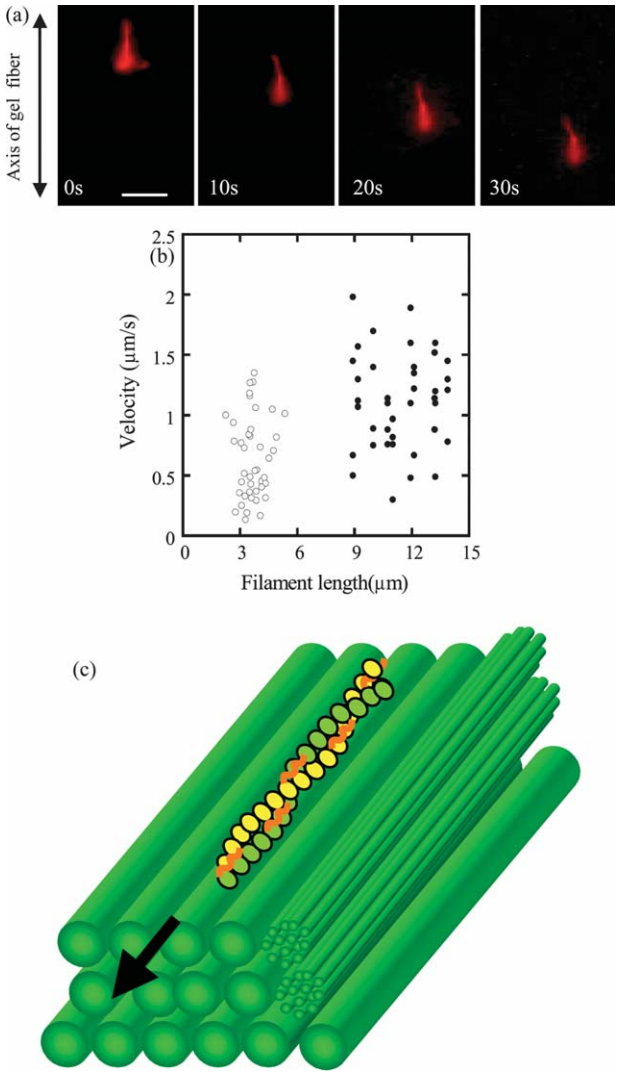

Fig. 8. Chemically cross-linked *p*-Lys-actin complex gel moves with the same speed as native F-actin on oriented myosin gel. (a) Sequential fluorescent images of the movement of *p*-Lys-actin gel on the oriented myosin gel. (b) Individual velocities of native F-actins (opened circle) and *p*-Lys-actin gels (closed circle) of various length on the oriented myosin gel. (c) Schematic illustration of the *p*-Lys-actin gels movement on the myosin gel. DA = 2.2 for the *p*-Lys-actin gels and DA = 1.7 for native F-actins. Scale bar: 50 μm ([12]).

the native F-actin, moves on the covalently cross-linked myosin gel, with an increased velocity. These results indicate that actins can be tailored into the desired shape and size without sacrificing their bioactivities by using complex formation with synthetic polymers.

However, the polarity of polymer–actin complexes, which is considered to be essential element in the sliding motion of polymer–actin complex gel, has not been clarified yet. This question is important for understanding the cooperative motion by actin assembly. In Section 3.5 we will describe the polarity of complexes formed in the presence of polycations and elucidate the correlation between the complex polarity and its motility on myosin.

3.5. Polarity and motility of polymer–actin complex gel [15]

An arrowhead-like pattern can be observed under transmission electron microscopy (TEM) when HMM was decorated on native F-actin (Fig. 9(a)), indicating that F-actin has a well-defined polarity by self-organization. The pointed end of arrowhead and the opposite end of arrowhead are called the p-end and b-end, respectively. To evaluate the polarity of actin complexes, we also attempted to decorate the actin complexes with HMM by the same method used

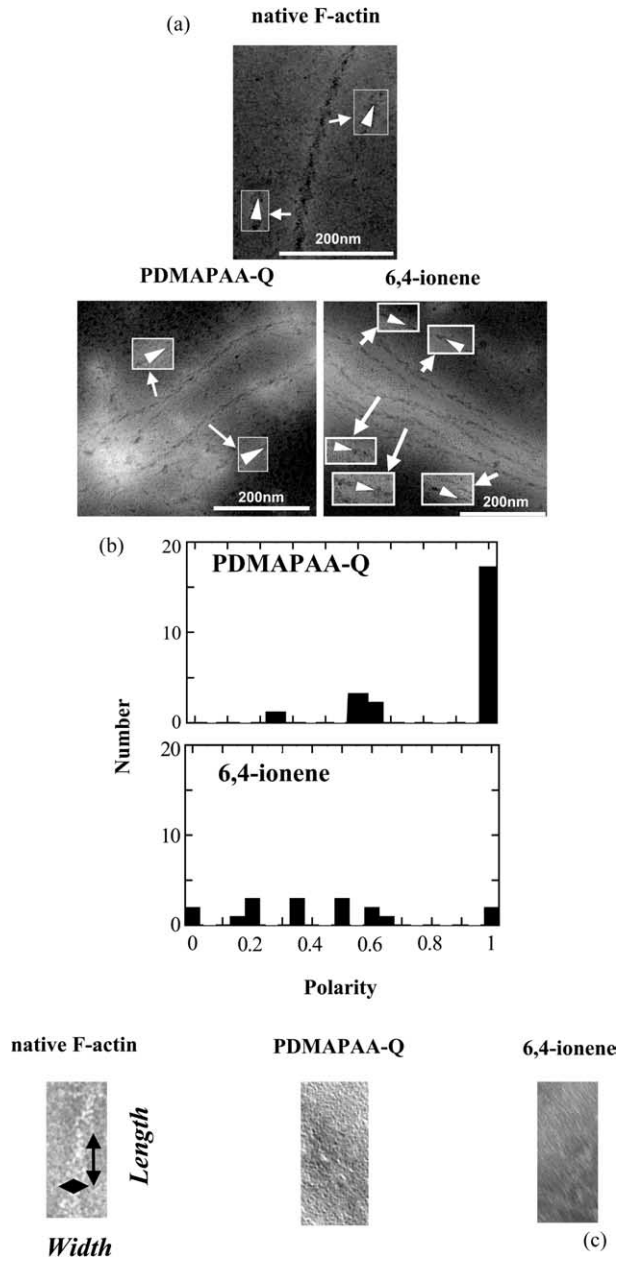

Fig. 9. (a) Polarity of polymer–actin complexes decorated with HMM. White arrows indicate the direction of arrowhead structures of decorated filaments. (b) Histograms of complex polarity distributions. (c) Enlarged images of arrowhead structures of F-actin and various polymer–actin complexes ([15]).

for F-actin. However, HMM was decorated only on the surface of the complex. Besides, the surface of the complexes was covered with myosin aggregates that are expected to be formed with extra polycations existing in the buffer solution. By adding polystyrene particles of 1.053 μm in diameter, we successfully removed the extra polycation and obtained clear arrowhead images of actin complexes decorated with HMM. Fig. 9(a) shows some examples of TEM images of HMM-decorated PDMAPAA-Q-actin complexes and 6,4-ionene-actin complexes. Different from native F-actin that is a single strand, the polymer–actin complexes are bundles that consist of 3–20 filaments. Arrowhead structures within a filament of the bundle pointed in the same direction, although some defects are observed occasionally. However, arrowhead directions of filaments within a bundle are not completely the same. The complex polarity defined by Eq. (1) was estimated. Fig. 9(b) shows the histograms of complex polarity distributions. As shown in Fig. 9(b), PDMAPAA-Q complexes show a preferential polarity. In contrast to this, distribution of 6,4-ionene complexes is isotropic. The average polarity of the actin complex is shown in Table 2. As shown in Table 2, polarity depends on the chemical structure of polycations, and PDMAPAA-Q-actin complex shows the highest polarity as 0.89 (average over 23 samples), while 6,4-actin shows the lowest value as 0.42 (average over 17 samples). Thus, PDMAPAA-Q prefers to form actin filament bundle having a unipolarity. These results show that actin and polycation form complexes with a preferential polarity.

Fig. 9(c) shows the enlarged images of arrowhead structures of F-actin and various polymer–actin complexes. We find that the arrowhead structure differs for different polymers. Table 3 summarizes the average arrowhead length and width of polymer–actin complexes. The average length and width of the arrowhead structure of native F-actin are 29.8 and 23.1 nm with a standard deviation of 6.6 and 3.4 nm, respectively. However, the length of the arrowhead structure of the *p*-Lys-actin complex and PDMAPAA-Q-actin complex is elongated and reaches as long as 44.5 and 40.5 nm with a standard deviation of 7.6 and 1.2, which is about 1.5 times and 1.3 times longer than that of native F-actin, respectively. On the other hand, average length and width of the arrowhead structure of the 6,10-ionene-actin complex is 24.2 and 17.5 nm with a standard deviation of 1.7 and 2.8, respectively, smaller than that of native F-actin. The change of the arrowhead structure might be attributed to the change of the helix pitch of a *p*-actin. *p*-Lys and PDMAPAA-Q are polycations carrying charges on their side chains. On the other hand, *x*,*y*-ionene is a polycation carrying charges on its main chain. The high flexibility of cations on the side chain of *p*-Lys and PDMAPAA-Q might account for the well-defined polarity of the complexes formed by actin and these polymers.

Table 2
Polarities of polymer–actin complexes

Polymer	Polarity
PDMAPAA-Q	0.89 ($n=23$)
p-Lys	0.76 ($n=21$)
3,3-Ionene	0.50 ($n=22$)
6,4-Ionene	0.42 ($n=17$)
6,10-Ionene	0.49 ($n=22$)

n is the number of samples for the average ([15]).

Table 3
Characteristic sizes of arrowhead structures of native actin and polymer–actin complexes ([15])

Polymer	Length (nm)	Width (nm)
Native actin	29.8±6.6	23.1±3.4
PDMAPAA-Q	40.5±2.3	21.9±1.2
p-Lys	44.5±7.6	24.8±3.8
3,3-Ionene	28.7±4.5	21.1±3.3
6,4-Ionene	25.3±3.1	18.1±1.9
6,10-Ionene	24.2±1.7	17.5±2.8

As reported in the above section, we have already elucidated that chemically cross-linked *p*-Lys-actin complex gels have an ability to slide on glass surfaces coated with immobilized myosin. To examine whether actin complex gels with PDMAPAA-Q and *x*,*y*-ionene bromide polymers ($x=3$ or 6; $y=3$, 4, or 10) could slide on the surface of myosin, the motility assays of PDMAPAA-Q-actin complex gels and *x*,*y*-ionene-actin complex gels in the presence of 4 mM ATP were performed. We found that all these polymer–actin complex gels show a sliding motion. Fig. 10 shows images of the PDMAPAA-Q-actin gel in sliding. The average velocities of the PDMAPAA-Q- and 3,3-, 6,4-, and 6,10-ionene-actin complex gels, calculated from the mean displacement in 3.3 s over 17–39 samples, were 1.3, 0.69, 0.48, and 0.79 μm/s with standard deviations of 0.63, 0.37, 0.38, and 0.41 μm/s, respectively, which are comparable with those of native F-actin (0.77 μm/s with a standard deviation of 0.32 μm/s). Among all these polymer–actin complexes, the PDMAPAA-Q-actin complex, which has the highest polarity, also shows the highest motility with a velocity of 1.3 μm/s. Dendritic complexes, which are occasionally observed when F-actin is mixed with 6,4-ionene, did not exhibit a translational motion but instead migrate around their barycentric position.

As shown in Fig. 11, a linear relationship between polarity and velocity at 3.3 s was observed, i.e. the velocity of the complex is proportional to the polarity. These results

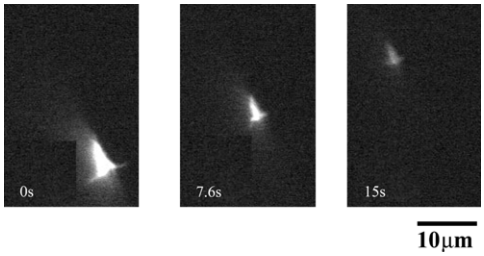

Fig. 10. Images of sliding motion of the PDMAPAA-Q-actin complex gel on myosin. The numbers in images are time in seconds ([15]).

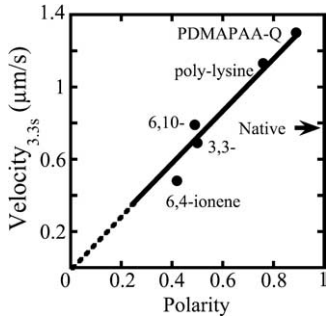

Fig. 11. Relationship between the polarity and the sliding velocity as determined by a time interval of 3.3 s for polymer–actin complex gels. Velocity data are the average over 17 samples. The velocity of a native F-actin is shown by the arrow in the figure ([15]).

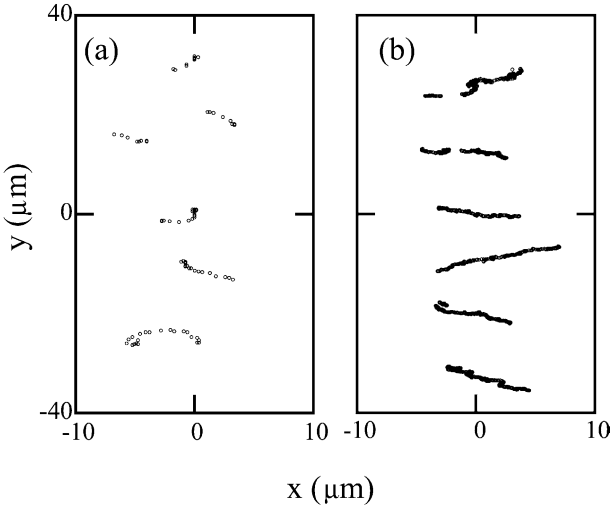

Fig. 12. Trajectories of sliding motion of native F-actin (a) and *p*-Lys-actin gel (b) on myosin. The position of trajectories is arbitrary. The time intervals of the plot of native F-actin and *p*-Lys-actin gel are 0.4 and 0.03 s, respectively ([15]).

suggest that the polarity of the polymer–actin complex is essential in producing a high motility. It is known that a native F-actin always moves toward one direction without moving back to the opposite direction. The direction of the F-actin motion is associated with its polarity [27]. For the polymer–actin bundles that are assembly of F-actin, the whole polarity is determined by the polar direction of F-actin. If the F-actin filaments assemble in an antiparallel way, the whole polarity is cancelled and leads no sliding motion. This explains why the correlation between polarity and velocity is observed.

However, the difference between the velocity of native F-actin and that of the polymer–actin complex gel with a polarity close to 1 (*p*-Lys-actin and PDMAPAAQ-actin) cannot be explained only in terms of polarity. The higher velocity observed for the complex gel should, therefore, be attributed to two possible factors: (1) the arrowhead structure and (2) the bundle formation. As shown in Fig. 9(c) and Table 3, the two gels, *p*-Lys-actin and PDMAPAAQ-actin, show an elongated arrowhead structure in comparison with the native F-actin and other polymer–actin complexes. If the change of the arrowhead structure is attributed to the change of the helix pitch of an actin filament, an elongation of arrowhead pattern will cause the extensions of helix structure of the actin filament. In consequence, the elasticity of the actin filament might increase and cause the effective motion.

On the other hand, by forming an actin bundle, the bending fluctuation is eliminated, and this also favors an effective motion. To elucidate the randomness of the motion, we investigate the trajectory of the motion. Fig. 12 shows the trajectory of native F-actin (Fig. 12(a)) and the *p*-Lys-actin complex (Fig. 12(b)) on the surface of myosin. One can see that the *p*-Lys-actin complex not only moves for a longer distance but also shows a more linear motion along its filament axis. To characterize the sliding motion, the displacement (d) of polymer–actin complex gels and native F-actin was plotted on a logarithmic scale as a function of observation time (t) (Fig. 13). Data are an average over 17 samples. The displacement (d) increases with the increase in the observation time (t) and follows a power law as $d \propto t^{\beta}$. The exponent β characterizes the motion. $\beta = 0.5$ corresponds to random motion, while $\beta = 1$ indicates constant linear translational motion. The β values for *p*-Lys-, PDMAPAA-Q-, and 3,3-, 6,4-, 6,10-ionene-actin complexes, and native actin filament were 0.81, 0.90, 0.82, 0.71, 0.84, and 0.69, respectively (Table 4). From this characterization, it is found that all polymer–actin complexes show more translational motion than that of native F-actin. Because polymer–actin complexes are bundles formed from actin filaments, they are less flexible than native F-actin. The less random motion of polymer–actin complexes is attributed to the less structural flexibility.

Previous studies of actin molecule motion on the glass surface coated with mysion showed that the sliding velocity is proportional to the probability, f, that one motor exerts the sliding force. f is expressed as $f = \tau_s/\tau_c$, where, τ_s and τ_c are the time the sliding force is exerted on actin and the cyclic

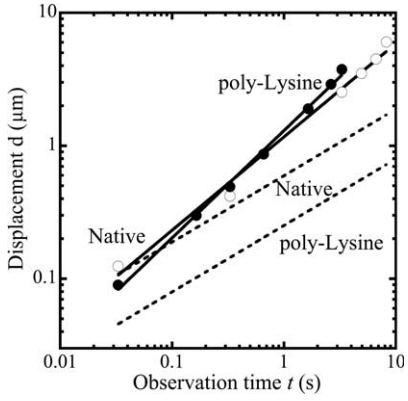

Fig. 13. Logarithmic plot of displacement (d) of *p*-Lys-actin gel (●) and native F-actin (○), as a function of observation time (t). The solid lines are experimental observations, and the dotted lines are theoretical values supposing a Brownian motion ([15]).

Table 4
Exponents β of native actin and polymer–actin complexes ([15])

Polymer	Native	PDMAPAA-Q	*p*-Lys	3,3-Ionene	6,4-Ionene	6,10-Ionene
β	0.69	0.90	0.81	0.82	0.71	0.84

time of ATP hydrolysis, respectively [28,29]. The factor that a highly oriented actin bundles show a higher sliding velocity than that of a single actin filament indicates that if many motors act on the same actin bundle, fluctuation which is associated to the stochasticity of the motor is negligible.

It should be emphasized that the sliding motion observed here is different from Brownian motion. Sliding motion occurs two-dimensionally on the surface of the motor protein of myosin, whereas Brownian motion is three-dimensional thermal diffusion. It is tempting to make a comparison between the sliding velocity driven by the chemical energy of ATP and the diffusion velocity arising from thermal agitation. We estimate the diffusion coefficient, D, of the actin bundle gel and native actin filament using the theory for stiff rods model [30]:

$$D = \frac{k_B T}{2\pi\eta_s L_C} \ln\frac{L_C}{b} \quad (3)$$

where $b = 12.1$ and 25.3 nm are the average diameter of the native F-actin and actin bundle gel, respectively. $L_C = 2.13$ and 7.22 μm are the average contour lengths of the native F-actin and actin bundle gel, respectively, which are estimated from TEM and scanning electron microscopy images. k_B is the Boltzmann constant, T is the temperature, and is the viscosity of the buffer. The diffusion coefficients of the native F-actin (D_a) and actin bundle gel (D_g) estimated from Eq. (3) are 18.8×10^{-14} and 6.08×10^{-14} m^2/s, respectively. As a result of its larger size of actin bundle gel, the D_g is about 1/3 of the D_a; that is, native actin filament can diffuse a $3^{0.5}$ times longer distance per unit time, as shown in Fig. 13. For an observation time longer than 1 s, for example, the actin bundle gel moves with velocity about 1 order of magnitude faster than that of the thermal diffusion.

Acknowledgements

This research is financially supported by PRESTO, JST and the Ministry of Education, Science, Sports, and Culture, Japan (Grand-in-Aid of Creative Scientific Research).

References

[1] Huxley HE. The mechanism of muscular contraction. Science 1969; 164:1356–65.
[2] Huxley AF. Reflections on muscle. Liverpool: Liverpool University Press; 1980.
[3] Pollack GH. Cells, gels and the engines of life. Seattle, WA: Ebner and Sons Publishers; 2001.
[4] Kitamura K, Tokunaga M, Iwane AH, Yanagida T. A single myosin head moves along an actin filament with regular steps of 5.3 nanometres. Nature 1999;397:129–34.
[5] Osada Y, Okuzaki H, Hori H. A polymer gel with electrically driven motility. Nature 1992;355:242–4.
[6] Mitsumata T, Ikeda K, Gong JP, Osada Y. Solvent-driven chemical motor. Appl Phys Lett 1998;73:2366–8.
[7] Osada Y, Matsuda A. Shape memory in hydrogels. Nature 1995;376: 219.
[8] Osada Y, Ross-Murphy SB. Intelligent gels. Sci Am 1993;268:82–7.
[9] Jager EWH, Smela E, Inganas O. Microfabricating conjugated polymer actuators. Science 2000;290:1540–6.
[10] Beebe DJ, Moore JS, Bauer JM, Yu Q, Liu RH, Devadoss C, et al. Functional hydrogel structures for autonomous flow control inside microfluidic channels. Nature 2000;404:588–90.
[11] Quake SR, Scherer A. From micro-to nanofabrication with soft materials. Science 2000;290:1536.
[12] Kakugo A, Sugimoto S, Gong JP, Osada Y. Gel machines constructed from chemically cross-linked actins and myosins. Adv Mater 2002; 14(16):1124–6.
[13] Kakugo A, Shikinaka K, Matsumoto K, Gong JP, Osada Y. Growth of large polymer–actin complexes. Bioconjugate Chem 2003;14(6): 1185–90.
[14] Kakugo A, Sugimoto S, Shikinaka K, Gong JP, Osada Y. Characteristics of chemically cross-linked myosin gels. J Biomater Sci Polymer Ed, 2005;16(2):2003–18.
[15] Kakugo A, Shikinaka K, Takekawa N, Sugimoto S, Osada Y, Gong JP. Polarity and motility of large polymer–actin complexes. Biomacromolecules, 2005;6:845–49.
[16] Spudich JA, Watt S. The regulation of rabbit skeletal muscle contraction. J Biol Chem 1971;246:4866–71.
[17] Barany M, Barany K. Myosin from the striated adductor muscle of scallop. Biochem Z 1966;345:37–56.
[18] Craig R, Szent-Gyorgi AG, Beese L, Flicker P, Vibert P, Cohen C. Electron microscopy of thin filaments decorated with a Ca2+-regulated myosin. J Mol Biol 1980;140:35–55.
[19] Younburg GE, Youngburg MN. Phosphorous metabolism I. A system of blood phosphorus analysis. J Lab Clin Med 1930;16:158–66.
[20] Uyeda TQP, Warruch HM, Korn SJ, Spudich JA. Quantized velocities at low myosin densities in an in vitro motility. Nature 1991;352: 307–11.
[21] Huxley HE. Sliding filaments and molecular motile systems. J Biol Chem 1990;265:8347–50.
[22] Korn SJ, Spudich JA. Fluorescent actin filaments move on myosin fixed to a glass surface. Proc Natl Acad Sci USA 1986;83:6272–6.
[23] Brown SS, Spudich JA. Nucleation of polar actin filament assembly by a positively charged surface. J Cell Biol 1979;80:499–504.
[24] Hayakawa K, Santerre JP, Kwak JC. Study of surfactant–polyelectrolyte interactions. Binding of dodecyl- and tetradecyltrimethylammonium bromide by some carboxylic polyelectrolytes. Macromolecules 1983;16:1642–5.
[25] Gong JP, Mizutani T, Osada Y. A comparative study on the cooperative binding of surfactants with solubilized polymers and networks. Polym Adv Technol 1996;7:797–804.
[26] Satake I, Yang JT. Interaction of sodiumdecyl sulfate with poly (L-ornithine) and poly (L-lysine) in aqueous solution. Biopolymers 1976; 15:2263–75.

[27] Pollack GH. Cells, gels and the engines of life. Seattle, WA: Ebner and Sons Publishers; 2001.
[28] Uyeda TQP, Korn SJ, Spudich JA. Myosin step size estimation from slow sliding movement of action over low densities of heavy meromyosin. J Mol Biol 1990;214:699–710.
[29] Harada Y, Sakurada K, Aoki T, Thomas DD, Yanagida T. Mechanochemical coupling in actomyosin energy transduction studied by in vitro movement assay. J Mol Biol 1990;216:49–68.
[30] Doi M, Edwards SF. The theory of polymer dynamics. 2nd ed. Oxford: Pergamon; 1980.